



Article

Resistance Coefficient Estimation for a Submarine's Bare Hull Moving in Forward and Transverse Directions

Hassan Saghi ^{1,2} , Joško Parunov ^{1,*}  and Antonio Mikulić ¹ ¹ Faculty of Mechanical Engineering and Naval Architecture, University of Zagreb, 10000 Zagreb, Croatia² Department of Civil Engineering, Hakim Sabzevari University, Sabzevar 9617976487, Iran

* Correspondence: jparunov@fsb.hr

Abstract: Resistance of the bare hull of the tourist submarine with spherical heads, moving in forward and transverse directions is analyzed in OpenFOAM using Computational Fluid Dynamics. The resistance coefficients of the submarine are estimated for different length-to-diameter ratios and Reynolds numbers. The Artificial Neural Network with the optimum number of neurons is then trained to predict the resistance coefficients. Two simplified Artificial Neural Network models and Nonlinear Least Squares Marquardt-Levenberg algorithm are employed to fit the results in the form of equations that may be used in the initial design of this type of submarines. The comparative analysis of different prediction models is performed and guidelines for their practical application are given.

Keywords: submarine; resistance coefficient; Artificial Neural Network; Nonlinear Least Squares Marquardt-Levenberg algorithm; Computational Fluid Dynamics



Citation: Saghi, H.; Parunov, J.; Mikulić, A. Resistance Coefficient Estimation for a Submarine's Bare Hull Moving in Forward and Transverse Directions. *Appl. Sci.* **2022**, *12*, 10953. <https://doi.org/10.3390/app122110953>

Academic Editor: Fabio La Foresta

Received: 5 September 2022

Accepted: 25 October 2022

Published: 28 October 2022

Publisher's Note: MDPI stays neutral with regard to jurisdictional claims in published maps and institutional affiliations.



Copyright: © 2022 by the authors. Licensee MDPI, Basel, Switzerland. This article is an open access article distributed under the terms and conditions of the Creative Commons Attribution (CC BY) license (<https://creativecommons.org/licenses/by/4.0/>).

1. Introduction

The present study is inspired by the tourist submarine with the transparent acrylic hull, designed to provide visitors a view of the surrounding ocean in a comfortable manner [1,2]. The overall length of the studied submarine is about 25 m, while the external diameter of the acrylic hull is 2.64 m. The hull of the submarine has spherical heads on the ends, where one head is made of steel, while the other one has large acrylic dome to provide visibility to the pilot of the submarine. The specific feature of tourist submarines is their ability to move in different directions with low speed, while the power requirements are a central consideration in their design to maximize the cruising duration. Although power reduction can be achieved in different ways, e.g., by adopting energy-saving propulsion systems or controlling the boundary layer on the submarine's surface, the shaping of the submarine's hull is considered as the most efficient approach. So, the purpose of the present paper is twofold:

1. To develop accurate and efficient numerical hydrodynamic model for the resistance coefficient of the submarine moving in forward and transverse directions.
2. To develop prediction tool for the resistance coefficients of the submarine in the initial design phase, without need to perform complex hydrodynamic analysis.

Hydrodynamic calculations are performed by the numerical model in OpenFOAM, using Computational Fluid Dynamic (CFD). Practical engineering tool replacing hydrodynamic computations is developed using the Artificial Neural Network (ANN) with optimal number of neurons. As designers of marine structures may be disinclined for using ANN as a "black box", relatively simple design equations are proposed using two ANN models with small number of neurons, and by Nonlinear Least Squares Marquardt-Levenberg algorithm. Although the actual resistance coefficient of the tourist submarine is higher because of the appendices and additional structures, there is a great need to have preliminary estimate of the bare hull resistance, which is the main benefit of the present study [2].

The paper is organized as follows. In the second part of Introduction, literature review regarding hydrodynamic analysis of submarines and combinations of physics with neural networks is provided. After the explanation of the governing equations and boundary conditions in the second section, the developed model was validated in the third section. Section 4 presents the results and comparative analysis of different prediction models for the resistance coefficients. Finally, the conclusions are presented in Section 5.

Literature Review

Among the key aspects of naval architecture is predicting the resistance of ships and submerged bodies. In this regard, Reynolds Averaged Navier Stokes Equations (*RANS*) based solutions were studied broadly in the literature. Larsson et al. [3] compared the results for benchmark vessels investigated by various institutions and universities with codes implementing *RANS*. Wang et al. [4], investigated resistance and wave patterns of a submarine model at different depths, and the influence of free surface on the resistance was discussed. Moonesun et al. [5] studied flow behavior on a model of an underwater vehicle with a tango-shaped nose and presented some formulas for the resistance of submarine bare hulls in deep water. Lastly, they compared the equation to determine the optimum resistance coefficient for the submarine.

Sukas et al. [6] applied *RANS*-based *CFD* to the numerical simulation of the flow field around a surface piercing and a fully submerged body to estimate the total resistance of the submarine. A *CFD* analysis was presented by Moonesun et al. [7] on the bare hull form of submarines or torpedoes to minimize resistance. They studied the bare hull form without free surface effect since the required power will always be estimated for submerged navigation. *CFD* was used by Ahmed [8] to determine the viscous resistance of a tourist submarine suitable for work in the Red Sea region. In that study, the resistance and hydrodynamic characteristics of the flow surrounding the tourist submarine under different speeds were investigated using the finite volume *RANS* code *CFX*. Shen et al. [9] used model-scale submarine resistance tests to predict full-scale resistance. It was assumed that the residual resistance coefficient is independent of the Reynolds number and is measured at the model-scale.

Utina et al. [10] evaluated experimentally and numerically the pressure and frictional force in the opposite direction of the mini submarine movement. Anh et al. [11] calculated the resistance coefficient of an exploratory submarine with a displacement of 6.8 tons moving forward, backward, diving, and rising in different directions. A full-scale SUBOFF model was investigated by Liu et al. [12] for different forward speeds, submerged positions, and fluid densities. They showed that the submarine hydrodynamic performance is significantly affected by the forward speed and submerged depth. Based on Star CCM+ fluid simulation software, the resistance coefficients under different submarine depths and speeds were calculated based on the specific resistance characteristics of submarines sailing near the surface by Chen et al. [13].

Combining physics models with neural networks has been used in fluid dynamics during the last few years [14–18]. As an example, convolutional neural networks were used by Takaaki et al. [14] to model the flow around a circular cylinder at 100 Reynolds numbers. Brenner et al. [17] used machine learning for advancing fluid mechanics. The authors demonstrated that the suggested model is likely to have a positive impact provided outcomes are held to the long-held critical standards that should guide flow physics research. In another research, Brunton et al. [18] reviewed the history and development of machine learning in fluid mechanics, as well as opportunities for the future. A discussion of fundamental machine learning methodologies and their use in understanding, modeling, optimizing, and controlling fluid flow was presented in that paper. The models in these studies were used as a “black box” without explicit equations to estimate unknown parameters.

2. Governing Equations and Boundary Conditions

In the present study, a submerged bare hull of a submarine was modeled in a viscous and incompressible fluid so that the fluid flow was considered turbulent. Accordingly, *RANS* are used as the governing equations [19]:

$$\nabla \cdot (\rho \underline{V}) = 0 \tag{1}$$

$$\frac{\partial}{\partial t} [\rho \underline{V}] + \nabla \cdot [\rho \underline{V} \underline{V}] = -\nabla p + \nabla \cdot [\underline{\tau} - \rho \underline{V}' \underline{V}'] + \underline{f}_b \tag{2}$$

The nomenclature is presented at the end of the paper. To solve the *RANS*, the Pressure Implicit Method with Pressure Linked Equations (*PIMPLE*) algorithm was applied. Different terms of the discretized equations, such as derivative terms, gradient parameters, Laplace derivative terms, and divergence terms, were discretized using 1st order implicit Euler, 2nd order centered Gauss linear, skewness corrected centered Gauss linear correction, and Upwind schemes, respectively [20]. Using block mesh and refinement techniques, a cylindrical domain was generated by using a Cartesian structured grid. Different boundary conditions summarized in Table 1 were used for the velocity, pressure, kinetic energy, and dissipate rate on the boundaries shown in Figure 1. According to Allmendinger [21], if the submarine moves at a depth greater than five times the diameter of its hull, the effect of surface and wave interactions can be ignored.

Table 1. Different boundary conditions used for different parameters.

Boundary	Velocity	Pressure	Kinetic Energy (<i>k</i>)	Dissipation Rate (ϵ)
Inlet	Fixed Value	Zero Gradient	Fixed Value	Fixed value
Outlet	Inlet Outlet	Fixed Value	Inlet Outlet	Inlet Outlet
Body around	Moving wall velocity	Zero Gradient	Wall Function	Wall function
	Symmetry	Symmetry	Symmetry	Symmetry

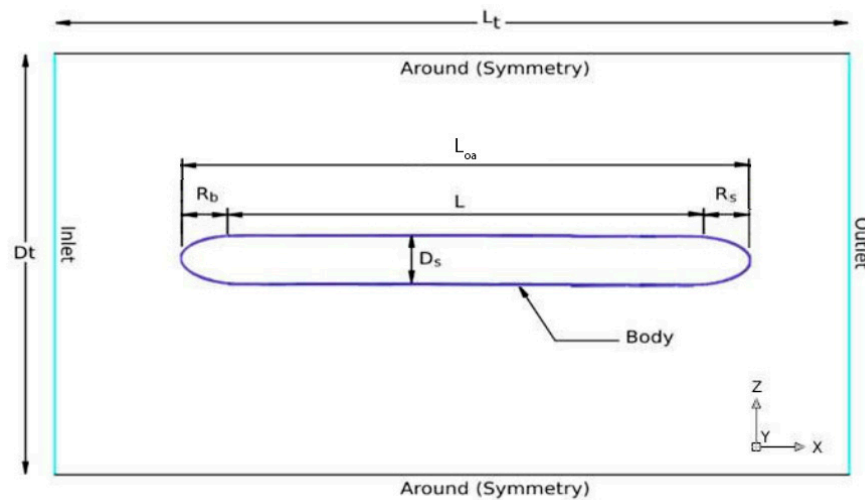


Figure 1. Schematic sketch of the domain and boundary conditions.

In addition, the *K-Epsilon* two-equation model was used to account for turbulence [22].

$$\frac{\partial}{\partial t} [\rho k] + \nabla \cdot [\rho \underline{V} k] = \nabla \cdot [\mu_{eff,k} \nabla k] + P_k - \beta \rho k \epsilon \tag{3}$$

$$\frac{\partial}{\partial t} [\rho \epsilon] + \nabla \cdot [\rho \underline{V} \epsilon] = \nabla \cdot [\mu_{eff,\epsilon} \nabla \epsilon] + C_{\epsilon 1} \frac{\epsilon}{k} P_k - C_{\epsilon 2} \rho \frac{\epsilon^2}{k} \tag{4}$$

where

$$C_{\epsilon 1} = 1.44 C_{\epsilon 2} = 1.92 \beta = 0.09$$

$$\mu_{eff,k} = \mu + \frac{\mu_t}{\sigma_k} \quad \mu_{eff,\varepsilon} = \mu + \frac{\mu_t}{\sigma_\varepsilon} \sigma_k = 1.0\sigma_\omega = 1.3$$

The resistance force and coefficient were calculated by integrating pressure and shear stress over the surface of the submarine as follows [23]:

$$R = \int_S p n_x dA + \int_S \tau_{xy} n_y dA + \int_S \tau_{xz} n_z dA \tag{5}$$

$$C_R = \frac{R}{\frac{1}{2}\rho S V_f^2} \tag{6}$$

where S is the surface area of the submarine’s bare hull.

2.1. Artificial Neural Network (ANN)

The back propagation (BP) ANN is a multilayer feedforward ANN used for benchmarking prediction performance [24–26]. There are three layers in BP ANN: input, hidden, and output. Each hidden layer receives the input signal through the input layer, and finally, the output layer receives it. Error signals are sent back to the hidden layer and the input layer. After that, the gradient descent algorithm is applied to adjust the weight and threshold of each neuron so that the BP analogy output is close to the expected value (See Figure 2). The number of neurons in the hidden layer is selected by repeated experiments to optimize the performance of the neural network.

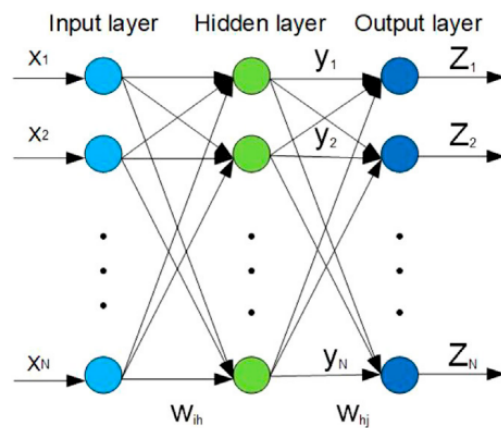


Figure 2. Structure of BP ANN (taken from [27]).

As ANN with many neurons can be used only as the “black box”, the approach may be inconvenient for submarine designers, who are usually not familiar with ANN. Therefore, it is of great practical interest to develop design equations for practical engineering usage. Since the equation derived from a neural network with many neurons would be very long and unusable, two ANN structures with one and two neurons in the hidden layer are considered (See Figures 3 and 4).

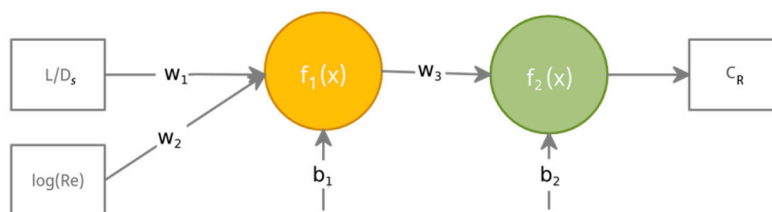


Figure 3. ANN structures with one neuron in the hidden layer.

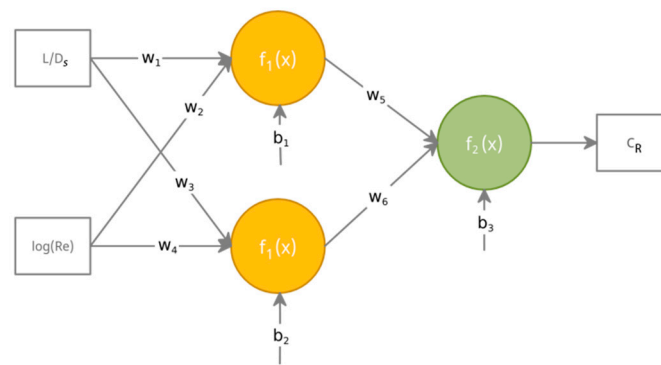


Figure 4. ANN structures with two neurons in the hidden layer.

Convolution produces the following output for the ANN shown in Figures 3 and 4, respectively:

$$C_R = f_2\left(b_2 + w_3 f_1\left(w_1 \frac{L}{D_s} + w_2 \log(R_e) + b_1\right)\right) \tag{7}$$

$$C_R = f_2\left(b_3 + w_5 f_1\left(w_1 \frac{L}{D_s} + w_3 \log(R_e) + b_1\right) + w_6 f_1\left(w_2 \frac{L}{D_s} + w_4 \log(R_e) + b_2\right)\right) \tag{8}$$

Activation functions introduce non-linearity into neural networks and help to capture the non-linear characteristics of input data [28,29]. There are different activation functions including Sigmoid, hyperbolic tangent, and Identity used in the neurons of the hidden and output layers of ANN [27]. According to the preliminary results of this study, ANNs with hyperbolic tangents ($f_1(x) = \tanh(x)$) and Identity ($f_2(x) = x$) activation functions in the hidden and output layers provides credible results.

2.2. Nonlinear Least Squares Levenberg-Marquardt Algorithm (NLLS)

Due to its high convergence efficiency to obtain the global optimal solution, the NLLS algorithm has been widely used [30–33]. By considering the equation $C_R = f\left(\frac{L}{D_s}, \log(R_e), p\right)$, the problem-solving nonlinear equations are expressed as:

$$F(x, p) = C_R - f\left(\frac{L}{D_s}, \log(R_e), p\right) \tag{9}$$

The nonlinear equation $f(x, p)$ needs to be solved, where x is the time series, y is the observations, and p is the nonlinear equation parameters. A nonlinear model is fitted by minimizing the sum of the square of errors, which can be expressed as:

$$\min \sum_{i=k}^n R - f\left(\frac{L}{D_s}, \log(R_e), p_k\right) = \min \sum_{i=k}^n \varepsilon_k \tag{10}$$

where p_k is the parameter of the k th iteration, and ε_k is the residual of the k th iteration. Taylor expansion was used to approximate the nonlinear function of $f(x, p_{k+1})$ for solving Equation (10) as follows:

$$f\left(\frac{L}{D_s}, \log(R_e), p_{k+1}\right) = f\left(\frac{L}{D_s}, \log(R_e), p_k + \Delta\right) = f(x, p_k) + J(p_k)\Delta \tag{11}$$

where J is the Jacobian matrix and Δ are the steps of the $(k + 1)$ th iteration. By solving the following equation, we can get the residual of the $(k + 1)$ th iteration as follows:

$$C_R - f\left(\frac{L}{D_s}, \log(R_e), p_{k+1}\right) = C_R - f\left(\frac{L}{D_s}, \log(R_e), p_k\right) - J(p_k)\Delta = \varepsilon_k - J(p_k)\Delta = 0 \tag{12}$$

It is known as Newton's method. This method, however, cannot be used to solve equations with overdetermined matrices. This problem was solved by multiplying a transposed matrix to reduce the overdetermined matrix's dimension by Gauss-Newton (Equation (13)).

$$J(p_k)^T J(p_k) \Delta = J(p_k)^T J(p_k) \varepsilon_k = g \quad (13)$$

By developing the Levenberg-Marquardt (LM) algorithm, the Gauss-Newton method was improved, since it does not work when the Hessian matrix is singular. To use the LM method, a constant, the trust-region radius, must be included in the equation as follows.

$$\Delta_k^{LM} = -\left(J(p_k)^T J(p_k) + \mu_k I\right)^{-1} g \quad (14)$$

The parameter μ_k is an iteration parameter introduced to overcome constraints caused by singularities or near singularities of $J(p_k)$. This parameter is also used to preventing Δ_k^{LM} from being too large when the Hessian matrix ($J(p_k)^T J(p_k)$) is nearly singular. Δ_k^{LM} is well defined in this case if μ_k is positive. In comparison to the steepest gradient method, Newton's method, and the Gauss-Newton method, the LM method is the most widely used nonlinear fitting method. Near to the solution, μ_k may be very small. In contrast, when the solution is far away, the value of μ_k may be very large; therefore, controlling μ_k can lead to an optimal solution.

3. Mesh Size Calibration

Figure 5a shows how a cube with $L_C = 0.45$ m edge length was placed inside a cylinder of 6 m length and 2 m diameter to determine mesh size. By considering the input boundary condition as a constant velocity, the total resistance of the cube against fluid flow is estimated. A cube was analysed against a constant 10 m/s fluid flow to examine the mesh size dependency. The numerical results showed that uniform mesh sizes (ms) with ms/L_C less than 0.09 did not significantly affect the total resistance as shown in Figure 5b.

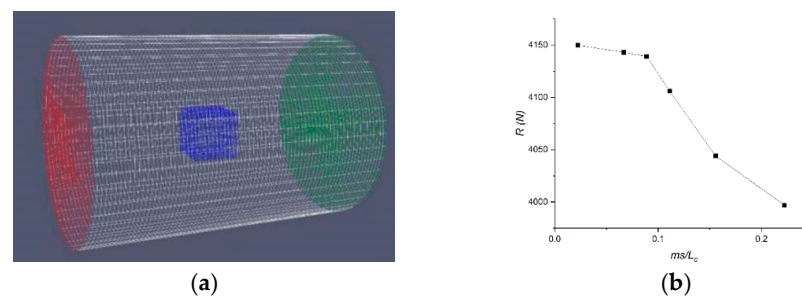


Figure 5. (a) The generated mesh of the cube inside a cylinder in OpenFOAM, (b) Mesh size dependence evaluation.

Accordingly, the developed model was used to estimate the resistance coefficient (C_R) of the cube by using Equation (15) against fluid flows with different velocities (V_f), and the results are shown in Figure 6a. Based on the results shown in Figure 6a, the average resistance coefficient for different speeds is calculated to be about 1.13. According to the literature [34–36], the resistance coefficient of a cube is estimated to be between 1.05 and 1.20. Therefore, the average of 1.13 was found to be in very good agreement with the amount suggested by other researchers.

$$C_R = \frac{2R}{\rho V_f^2 L^2} \quad (15)$$

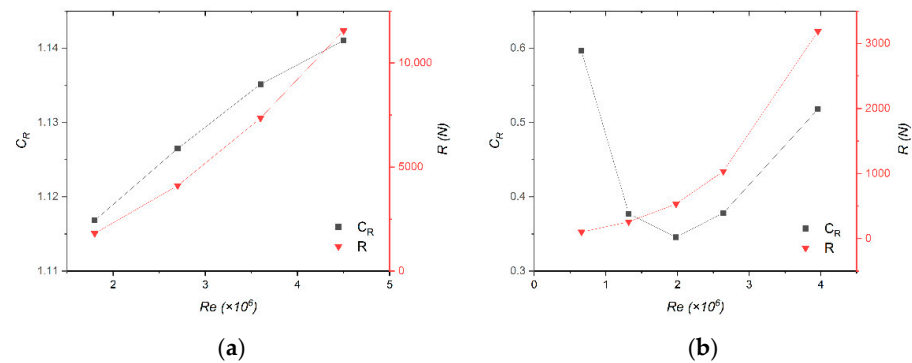


Figure 6. The resistance coefficient and total resistance of different geometries against fluid flowing at different Reynolds numbers (a) a cube of 0.45m length, (b) a sphere of 2.64 m diameter.

The cube exhibits significantly more vortex shedding than the submarine’s bare hull, so another mesh size verification is performed using the sphere. Thus, a sphere with a diameter of 2.64 m is also computed with the same mesh size. Figure 6b shows the resistance force and coefficient for fluid flows with different Reynolds numbers, where an average resistance coefficient of 0.45 was calculated. The resistance coefficient of a sphere is estimated in the range of 0.4 and 0.5 for Reynolds numbers greater than 10^4 [36]. Consequently, the average of 0.45 was found to be very close to the amount suggested in [37].

4. Results

The present study aims to model the bare hull of a submarine against speeds to derive equations for resistance coefficients in forward and transverse directions. To that end, a range of credible tourist submarine geometries, represented by the ratio L/D_S , is defined, and shown in Table 2, where L represents the length of the cylindrical hull, L_{oa} is the overall length including the heads, and D_S represents the diameter of the cylindrical hull. The geometries are defined by keeping the total internal volume of the submarine nearly constant. Isabella, a supercomputer housed at SRCE—University Computing Centre of the University of Zagreb, is used for the analysis. Isabella consists of 135 worker nodes, 3100 processor cores, 12 GPUs, and 756 TiB of data storage [38].

Table 2. The dimensions of a submarine for different L/D_S ratios.

Case	L (m)	D_S (m)	L/D_S
1	25	2.44	10.2
2	24	2.49	9.6
3	23	2.54	9.1
4	22	2.59	8.5
5	21.06	2.64	8.0
6	20	2.7	7.4
7	19	2.76	6.9
8	18	2.83	6.4
9	17	2.9	5.9

4.1. Forward Motion

A total of 117 different cases, as described in the previous section, were modeled in OpenFOAM for 13 different speeds (0.25, 0.35, 0.5, 0.6, 0.7, 0.8, 0.9, 1.0, 1.1, 1.2, 1.3, 1.4 and 1.5 m/s). Therefore, all 117 cases listed in Appendix A were analyzed. OpenFOAM computation for each of the 117 cases lasted for about 18,000 s, so the total running time was about 35,100 min. Results of the analysis were presented in Figure 6. The resistance coefficient for the forward motion in Figure 7 were presented against L/D_S and Reynolds number, given by the following expression:

$$Re_f = \frac{V_f D_S}{\nu} \tag{16}$$

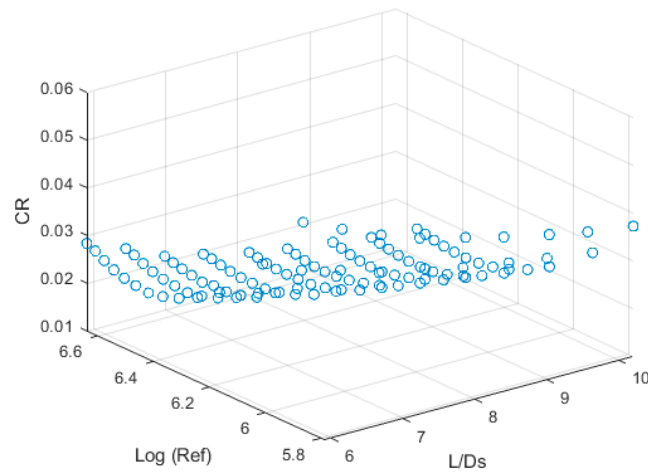


Figure 7. Variation of C_{R-f} versus the dimensionless parameters, L/D_S and $\log (R_{ef})$ for the forward direction.

In the present case, ν is the dynamic viscosity of $10^{-6} \frac{m^2}{s}$ [39].

The results shown in Figure 7 indicate that the relationship between the resistance coefficient in the forward direction (C_{D-f}) and L/D_S is almost linear. However, the change of this parameter is somewhat nonlinear at the low (e.g., 0.5 m/s) and high (e.g., 1.5 m/s) speeds. On the other hand, for all L/D_S , the relationship between C_{D-f} and forward speed (V_f) is nonlinear.

Next, *NLLS* and *ANN* methods were applied to fit the best curve to the results shown in Figure 7 and find a nonlinear equation to estimate the resistance coefficient of the bare hull based on two dimensionless parameters, L/D_S and Reynolds number (R_{ef}). The following equations were derived for the resistance coefficient of the submarine with the forward speed using the developed code in MATLAB. For the *ANN*, 70%, 15%, and 15% of data (corresponding to 83, 17, and 17 data) were used in training, testing, and evaluation steps, respectively:

NLLS:

$$C_{R-f} = 5.372 - 0.34 \frac{L}{D_S} + 1.625 \log(R_{ef}) + 0.0031 \left(\frac{L}{D_S}\right)^2 + 0.096 \frac{L}{D_S} \log(R_{ef}) + 0.125 \left(\log(R_{ef})\right)^2 - 0.0000534 \left(\frac{L}{D_S}\right)^3 - 0.0002102 \left(\frac{L}{D_S}\right)^2 \left(\log(R_{ef})\right) + 0.007171 \frac{L}{D_S} \left(\log(R_{ef})\right)^2 \tag{17}$$

ANN (Figure 3):

$$C_{R-f} = 0.0971 + 0.0827 \tanh\left(-0.146 \frac{L}{D_S} - 1.584 \log(R_{ef})\right) + 9.578 \tag{18}$$

ANN (Figure 4):

$$C_{R-f} = 0.112 + 0.0547 \tanh\left(-0.161 \frac{L}{D_S} + 1.971 \log(R_{ef}) - 13.066\right) + 0.047 \tanh\left(-0.119 \frac{L}{D_S} - 2.004 \log(R_{ef}) + 12.325\right) \tag{19}$$

To assess that accuracy of Equations (17)–(19), *ANNs* with larger number of neurons (*NON*) in the hidden layer (see Figure 8) are also trained.

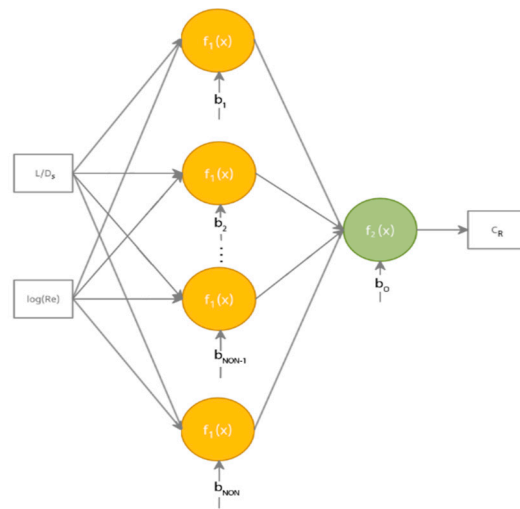


Figure 8. ANN structures with large NON in the hidden layer.

In ANN, the optimal NONs in the hidden layers is determined by trial and error and not straightforwardly. However, it was advised to use 2–4 times the input layer’s number of nodes [40,41]. So, by considering the number of nodes in the input layer = 2, ANNs with 3–10 neurons in the hidden layer (as a “black box”) were used to estimate the resistance coefficient of the submarine for the speeds of 0.1, 0.45, 1.15, and 1.7 m/s, and Sum Square Error ($SSE = ((C_{R-f})_{CFD} - (C_{R-f})_{Pre})^2$) of the models were estimated and shown in Figure 9. $(C_{R-f})_{CFD}$ and $(C_{R-f})_{Pre}$ are the predicted resistance coefficient by using CFD and ANN, respectively.

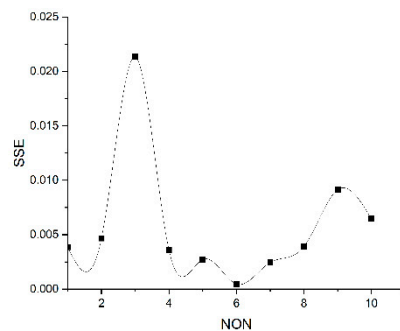


Figure 9. The SSE of ANN versus the NON for forward motion.

Figure 9 shows that ANN with six neurons in the hidden layer ($NON = 6$) has the best performance for predicting resistance coefficients.

Equations (17) to (19) and the trained ANN with $NON = 6$ were used to predict the resistance coefficient of the submarine for the speeds 0.1, 0.45, 1.15, and 1.7 m/s, and the results were shown in Figure 10. The error estimated as $Error = 100 * \frac{(C_{R-f})_{CFD} - (C_{R-f})_{Pre}}{(C_{R-f})_{CFD}}$ was also calculated for different methods and shown in Figure 11.

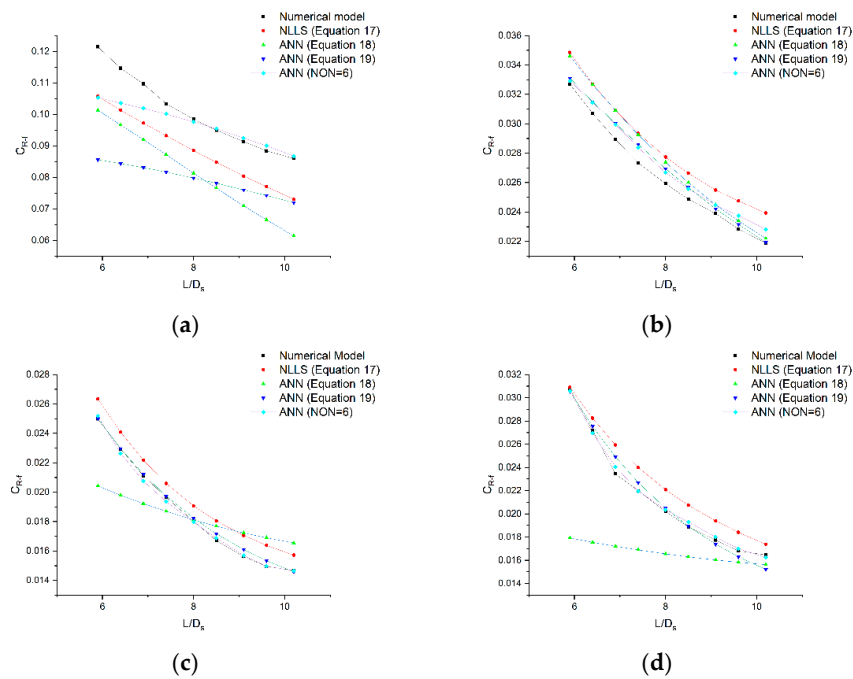


Figure 10. Comparison of the resistance coefficient of the different cases of the submarines for some forward speeds, (a) $V_f = 0.1$ m/s, (b) $V_f = 0.45$ m/s, (c) $V_f = 1.15$ m/s, (d) $V_f = 1.7$ m/s.

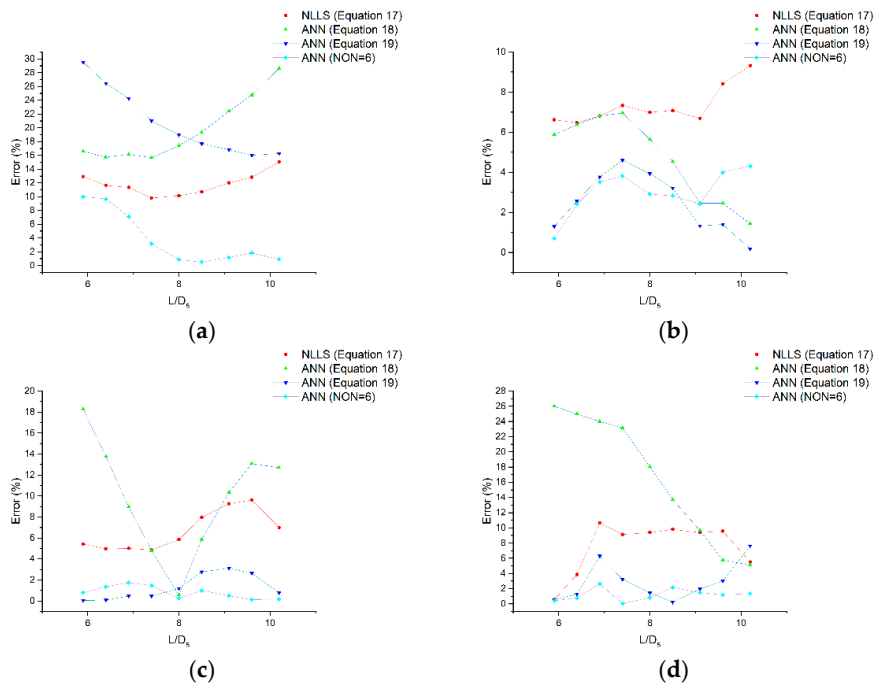


Figure 11. Comparison of the estimation error of the resistance coefficient of the different cases of the submarines for different forward speeds, (a) $V_f = 0.1$ m/s, (b) $V_f = 0.45$ m/s, (c) $V_f = 1.15$ m/s, (d) $V_f = 1.7$ m/s.

According to Figure 11a, Equations (18) and (19) are unable to estimate accurately the resistance coefficient for speeds lower than those used in training the artificial neural network. The model error varies from 15 to 30 percent depending on the submarine’s length and diameter. *NLLS* (Equation (17)) estimates the resistance coefficient with a maximum error of 15%. *ANN* with $NON = 6$ estimates the resistance coefficient with a maximum error of 3% and 10% for the submarines with $L/D_S > 7.5$ and $L/D_S < 7.5$, respectively.

As shown in Figure 11b,c, Equations (17) and (19) and ANN with $NON = 6$ provide high accuracy for estimating resistance coefficients at speeds used for training ANNs and NLLS.

The results for the forward speed 1.7 m/s (Figure 11d) which was higher than the range of speeds used in the extraction of relationships indicates that Equations (17) and (19) estimate the resistance coefficient with a maximum 10% and 7% error, respectively. ANN with $NON = 6$ shows a better performance than other methods, with maximum error of 3%.

4.2. Transverse Motion

Tourist submarines are equipped with transverse thrusters to enable transverse motion and maneuvering. Additionally, they are used to prevent the transverse motion by acting in the opposite direction to the sea current. Therefore, there is an interest in studying the transverse resistance of the submarine as well as the transverse motion of the submarine, and to suggest equations to estimate the resistance coefficient in the transverse direction. To accomplish this, 90 different cases are modeled in OpenFOAM using the developed code for 10 different transverse speeds (0.05, 0.10, 0.15, 0.20, 0.25, 0.30, 0.35, 0.4, 0.45 and 0.5 m/s). Therefore, 90 cases listed in Appendix B were analyzed and are shown in Figure 12. OpenFOAM computation for each of the 90 cases lasted for about 18,000 s, so the total running time was about 27,000 min.

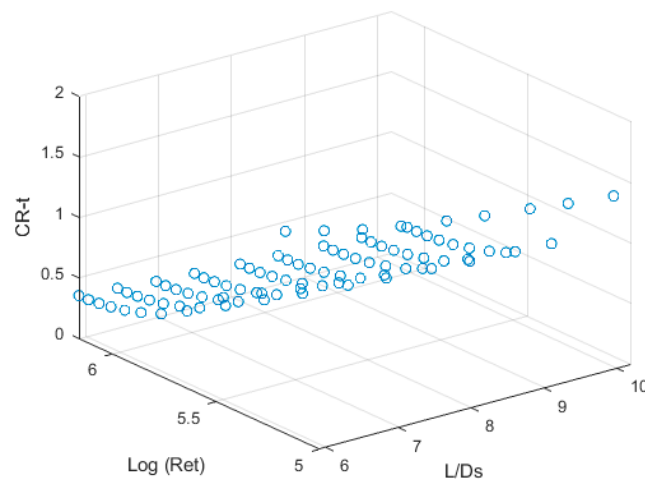


Figure 12. Variation of the resistance coefficient versus the dimensionless parameters, L/D_S and $\log(R_{et})$ for the transverse directions.

Figure 12 shows that the resistance coefficient in the transverse direction (C_{D-t}) is linearly related to the L/D_S . Nevertheless, for all L/D_S , the relationship between C_{D-t} and transverse speed (V_t) is nonlinear. NLLS and ANNs were applied to fit the best curve to the obtained results shown in Figure 13 and to find a nonlinear equation to estimate the resistance coefficient of the bare hull based on two dimensionless parameters, L/D_S and Reynolds number (R_{et}). The following equations were derived for the resistance coefficient of the submarine with transverse speed using the code in MATLAB. In ANN, 70%, 15%, and 15% of data (corresponding to 64, 13, and 13 data) were also used in training, testing, and evaluation steps, respectively:

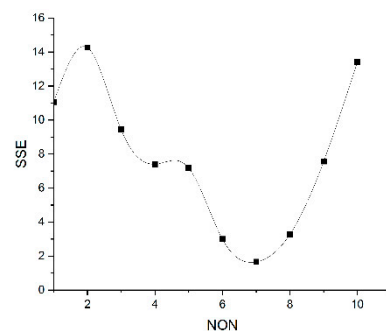


Figure 13. The SSE of ANN versus the NON for transverse motion.

NLLS:

$$C_{R-t} = 232.71 - 5.211889 \frac{L}{D_s} - 105.35826(\log(R_{et})) + 0.083091 \left(\frac{L}{D_s}\right)^2 + 1.46633 \frac{L}{D_s} (\log(R_{et})) + 16.000585(\log(R_{et}))^2 - 0.0133027 \left(\frac{L}{D_s}\right)^2 \log(R_{et}) - 0.101747 \frac{L}{D_s} (\log(R_{et}))^2 - 0.815011(\log(R_{et}))^3 \tag{20}$$

ANN (Figure 3):

$$C_{R-t} = 1.772 + 1.513 \tanh\left(-0.093 \frac{L}{D_s} - 1.92 \log(R_{et}) + 10.361\right) \tag{21}$$

ANN (Figure 4):

$$C_{R-t} = 1.516 + 1.22 \tanh\left(-0.1093 \frac{L}{D_s} - 2.278 \log(R_{et}) + 12.466\right) + 0.0374 \tanh\left(-0.534 \frac{L}{D_s} - 3.695 \log(R_{et}) + 26.177\right) \tag{22}$$

The data in Appendix B has also been used to train ANNs with more than two neurons in the hidden layer (see Figure 8). The resistance coefficient was estimated at 0.02 m/s as a test of the ability of the proposed models to estimate it at different speeds. This speed is lower and outside the range used for the extraction of relations. In addition, the resistance coefficient of the submarine at transverse speeds of 0.125 and 0.375 was estimated, which was included in the range of speeds used in the extraction of relationships, but not in the training. In a similar manner, the resistance coefficient was estimated for a speed of 0.6, which was higher than the range of speeds used to extract the relationships. Training ANNs with different NONs were used to predict the coefficient of resistance of the submarine at speeds of 0.02 m/s, 0.125, 0.375, and 0.6, and SSE is shown in Figure 13.

It is shown in Figure 13 that ANN with seven neurons in the hidden layer (NON = 7) performs the best at predicting resistance coefficients. So, Equations (20) to (22) and the trained ANN with NON = 7 were used to estimate the resistance coefficient at speeds of 0.02 m/s, 0.125, 0.375, and 0.6, and the results were shown in Figure 14. The estimation error for the resistance coefficient is shown in Figure 15.

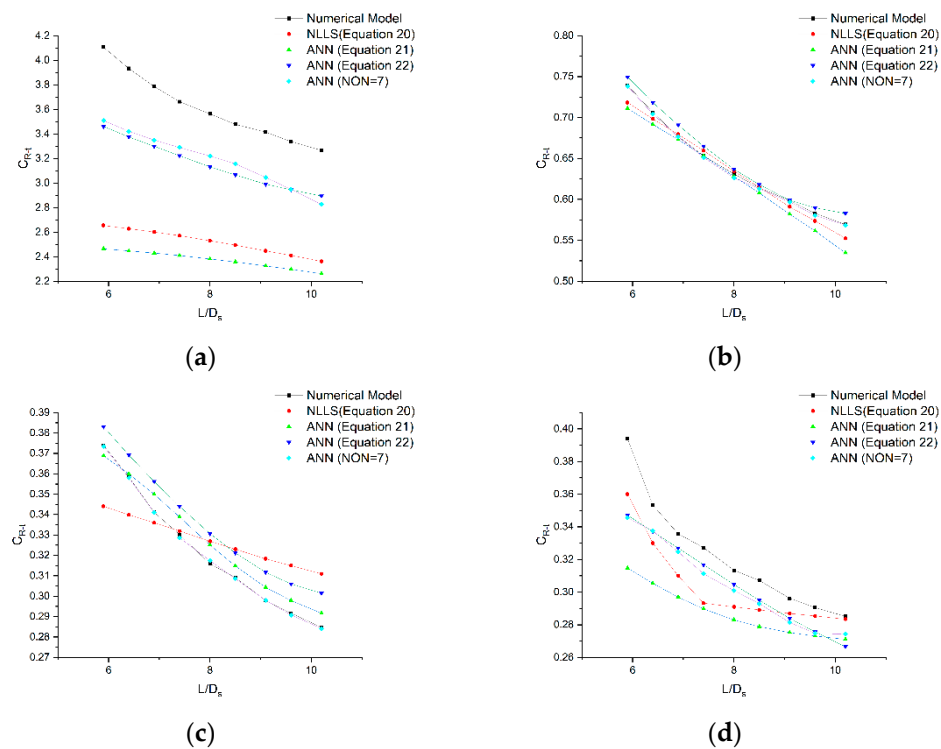


Figure 14. Comparison of the resistance coefficient of the different cases of the submarines for some transverse speeds, (a) $V_t = 0.02$ m/s, (b) $V_t = 0.1255$ m/s, (c) $V_t = 0.375$ m/s, (d) $V_t = 0.6$ m/s.

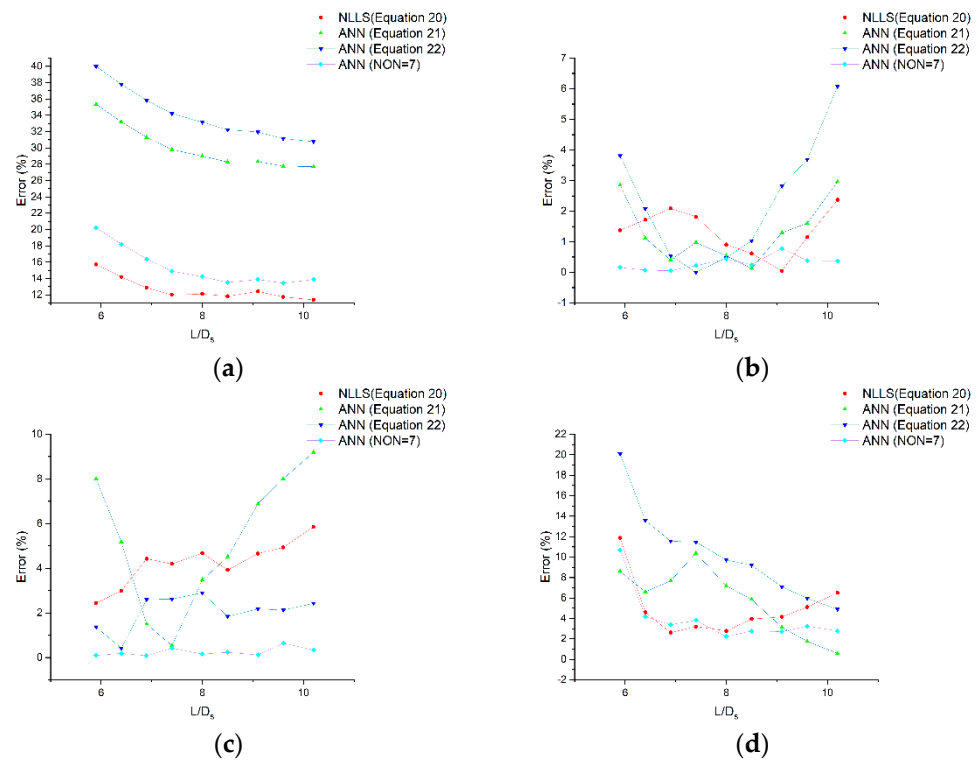


Figure 15. Comparison of the estimation error of the resistance coefficient of the different cases of the submarines for some transverse speeds, (a) $V_t = 0.02$ m/s, (b) $V_t = 0.1255$ m/s, (c) $V_t = 0.375$ m/s, (d) $V_t = 0.6$ m/s.

Figure 15a shows that the derived equations (Equations (21) and (22)) by using ANN are not able to estimate accurately resistance coefficients at lower speeds than those used in the ANN training, while the NLLS method (Equation (20)) can estimate the resistance coefficient for the transverse direction with a maximum error of 15%. Even ANN with $NON = 7$ is not performing well, having a maximum error of 20%.

As shown in Figure 15b,c, the proposed equations and ANN with $NON = 7$ are effective in estimating resistance coefficients at speeds inside the training range.

According to the results for 0.6 m/s transverse speed (Figure 15d), which is higher than the range of speeds used to extract relationships, Equation (21) can estimate resistance coefficients with a maximum of 10% for the submarine with $L/D_S > 7.5$, while Equation (20) shows maximum error of 12% in all cases. ANN with $NON = 7$ is slightly better, with 10% prediction error.

5. Discussion

The range of the estimation error is summarized in Table 3.

Table 3. The range of the estimation error (%) for the velocities below, within, and above those used for the training.

Parameter	Equation	Below the Range		Within the Range		Above the Range	
		$L/D_S > 7.5$	$L/D_S < 7.5$	$L/D_S > 7.5$	$L/D_S < 7.5$	$L/D_S > 7.5$	$L/D_S < 7.5$
C_{R-f}	Equation (17) (NLLS)	10–15	11–13	7–9	6–7	6–10	1–11
	Equation (18) (ANN)	15–30	16–17	1–13	6–18	5–23	24–26
	Equation (19) (ANN)	15–21	24–30	0.2–5	1–4	0.2–7	1–6
	ANN (NON = 6)	1–3	7–10	2–4	1–4	0.1–2	0.8–3

Table 3. Cont.

Parameter	Equation	Below the Range		Within the Range		Above the Range	
		$L/D_S > 7.5$	$L/D_S < 7.5$	$L/D_S > 7.5$	$L/D_S < 7.5$	$L/D_S > 7.5$	$L/D_S < 7.5$
C_{R-t}	Equation (20) (NLLS)	11–12	13–16	4–6	2–4	3–7	3–12
	Equation (21) (ANN)	28–30	31–30	1–9	2–8	1–10	7–9
	Equation (22) (ANN)	25–30	21–27	2–3	0.4–3	5–11	12–15
	ANN (NON = 7)	13–15	16–20	0.6–1	0.1–0.2	2–4	3–10

The following conclusions can be made on the accuracy of the procedures for estimating the resistance coefficient:

- For the velocities lower than the range used for training, ANN with NON = 6 shows much better ability to estimate the resistance coefficient for the forward direction compared to the equations. Surprisingly, for transverse movement the NLLS performs better than the ANN.
- For forward velocities higher than those used for the training, ANN with optimal NON has the lowest error. However, for transverse directions, differences between equations and ANN are small.
- For transverse velocities within training range, ANN with NON = 7 is more accurate than the equations. For forward motion, however error of Equation (19) is close to the error of ANN with NON = 6.

6. Conclusions

A Computational Fluid Dynamics numerical model in OpenFOAM is developed to compute the resistance coefficient of a tourist submarine's bare hull with a variable length-to-diameter ratio at different speeds, moving in forward and transverse directions.

To propose a practical design estimation method for hydrodynamic resistance of a submarine, the Artificial Neural Network is trained with optimal number of neurons, which is found to be 6 and 7 for forward and transverse direction, respectively. Furthermore, two simple Artificial Neural Network models with small number of neurons and Nonlinear Least Squares Marquardt-Levenberg algorithm are employed to develop design equations for the resistance of the bare hull in two directions. Although the proposed equations perform relatively well compared to the numerical results, the Artificial Neural Network with optimal number of neurons leads to the more reliable results in most of the cases. The care should be taken when employing Artificial Neural Network outside the training range, as large errors could arise, as shown in Table 3.

The actual resistance coefficient of the tourist submarine will be higher because of the appendages and external structures [2]. Nevertheless, equations and results developed herein may be used for preliminary estimate of the bare hull resistance, which is necessary step in evaluation of the total submarine's resistance.

Author Contributions: Conceptualization, J.P. and H.S.; methodology, H.S. and A.M.; software, H.S. and A.M.; validation, H.S. and A.M.; formal analysis, H.S.; investigation, H.S.; resources, J.P.; data curation, H.S.; writing—original draft preparation, H.S.; writing—review and editing, A.M. and J.P.; visualization, H.S. and A.M.; supervision, J.P.; project administration, J.P.; funding acquisition, J.P. All authors have read and agreed to the published version of the manuscript.

Funding: This research was funded by the European Union from the European Regional Development Fund within the Operational Program “Competitiveness and Cohesion 2014–2020”, project KK.01.2.1.02.0339—Development of the multipurpose luxury touristic and research submarine.

Acknowledgments: The project is co-financed by the European Union from the European Regional Development Fund within the Operational Program “Competitiveness and Cohesion 2014–2020”, project KK.01.2.1.02.0339—Development of the multipurpose luxury touristic and research submarine. The content of the publication is the sole responsibility of the project partner, the University of Zagreb, Faculty of Mechanical Engineering and Naval Architecture. This research was performed

using the resources of computer cluster Isabella based in SRCE—University of Zagreb University Computing Centre.

Conflicts of Interest: The authors declare no conflict of interest.

Nomenclature

Symbols

C_{R-f}	Resistance coefficient for the forward speed
C_{R-t}	Resistance coefficient for the transverse speed
D_S	Diameter of the submarine
L	Length of the parallel middle body of submarine
L_{oa}	Total length of submarine
Re_f	Reynolds number for the forward speed
Re_t	Reynolds number for the transverse speed
V	Velocity vector
V_f	Forward speed of the submarine
V_t	Transverse speed of the submarine
f_b	Body force
\overline{dx}	Mesh size in x direction
\overline{dy}	Mesh size in y direction
\overline{dz}	Mesh size in z direction
p	Dynamic pressure
t	Time
τ	Shear stress tensor
ρ	Fluid density
τ_{xy}	Shear stress in the plane xy
τ_{xz}	Shear stress in the plane xz
∇	Gradient operator

Abbreviations

ANN	Artificial Neural Network
BP	Back Propagation
CFD	Computational Fluid Dynamics
LM	Levenberg-Marquardt
NLLS	Nonlinear Least Squares Marquardt-Levenberg algorithm
NON	Number of neurons in the hidden layer of ANN
PIMPLE	Pressure Implicit Method with Pressure Linked Equations
RANSE	Reynolds Average Navier Stokes equations

Appendix A

Table A1. Various scenarios of the submarine at different speeds for the forward motion.

Case	L (m)	L_{oa} (m)	D_S (m)	L/D_S	V_f (m/s)	$\text{Log}(Re_f)$
1	25	27.44	2.44	10.2	0.25	5.79
2	24	26.49	2.49	9.6	0.25	5.79
3	23	25.54	2.54	9.1	0.25	5.80
4	22	24.59	2.59	8.5	0.25	5.81
5	21.06	23.7	2.64	8.0	0.25	5.82
6	20	22.7	2.7	7.4	0.25	5.83
7	19	21.76	2.76	6.9	0.25	5.84
8	18	20.83	2.83	6.4	0.25	5.85
9	17	19.9	2.9	5.9	0.25	5.86

Table A1. Cont.

Case	L (m)	L_{oa} (m)	D_S (m)	L/D_S	V_f (m/s)	$\text{Log}(R_{ef})$
10	25	27.44	2.44	10.2	0.35	5.93
11	24	26.49	2.49	9.6	0.35	5.94
12	23	25.54	2.54	9.1	0.35	5.95
13	22	24.59	2.59	8.5	0.35	5.96
14	21.06	23.7	2.64	8.0	0.35	5.97
15	20	22.7	2.7	7.4	0.35	5.98
16	19	21.76	2.76	6.9	0.35	5.98
17	18	20.83	2.83	6.4	0.35	6.00
18	17	19.9	2.9	5.9	0.35	6.01
19	25	27.44	2.44	10.2	0.5	6.09
20	24	26.49	2.49	9.6	0.5	6.10
21	23	25.54	2.54	9.1	0.5	6.10
22	22	24.59	2.59	8.5	0.5	6.11
23	21.06	23.7	2.64	8.0	0.5	6.12
24	20	22.7	2.7	7.4	0.5	6.13
25	19	21.76	2.76	6.9	0.5	6.14
26	18	20.83	2.83	6.4	0.5	6.15
27	17	19.9	2.9	5.9	0.5	6.16
28	25	27.44	2.44	10.2	0.6	6.17
29	24	26.49	2.49	9.6	0.6	6.17
30	23	25.54	2.54	9.1	0.6	6.18
31	22	24.59	2.59	8.5	0.6	6.19
32	21.06	23.7	2.64	8.0	0.6	6.20
33	20	22.7	2.7	7.4	0.6	6.21
34	19	21.76	2.76	6.9	0.6	6.22
35	18	20.83	2.83	6.4	0.6	6.23
36	17	19.9	2.9	5.9	0.6	6.24
37	25	27.44	2.44	10.2	0.7	6.23
38	24	26.49	2.49	9.6	0.7	6.24
39	23	25.54	2.54	9.1	0.7	6.25
40	22	24.59	2.59	8.5	0.7	6.26
41	21.06	23.7	2.64	8.0	0.7	6.27
42	20	22.7	2.7	7.4	0.7	6.28
43	19	21.76	2.76	6.9	0.7	6.29
44	18	20.83	2.83	6.4	0.7	6.30
45	17	19.9	2.9	5.9	0.7	6.31
46	25	27.44	2.44	10.2	0.8	6.29
47	24	26.49	2.49	9.6	0.8	6.30
48	23	25.54	2.54	9.1	0.8	6.31
49	22	24.59	2.59	8.5	0.8	6.32
50	21.06	23.7	2.64	8.0	0.8	6.32
51	20	22.7	2.7	7.4	0.8	6.33
52	19	21.76	2.76	6.9	0.8	6.34
53	18	20.83	2.83	6.4	0.8	6.35
54	17	19.9	2.9	5.9	0.8	6.37
55	25	27.44	2.44	10.2	0.9	6.34
56	24	26.49	2.49	9.6	0.9	6.35
57	23	25.54	2.54	9.1	0.9	6.36
58	22	24.59	2.59	8.5	0.9	6.37
59	21.06	23.7	2.64	8.0	0.9	6.38
60	20	22.7	2.7	7.4	0.9	6.39
61	19	21.76	2.76	6.9	0.9	6.40
62	18	20.83	2.83	6.4	0.9	6.41
63	17	19.9	2.9	5.9	0.9	6.42

Table A1. Cont.

Case	L (m)	L_{oa} (m)	D_S (m)	L/D_S	V_f (m/s)	$\text{Log}(R_{cf})$
64	25	27.44	2.44	10.2	1.0	6.39
65	24	26.49	2.49	9.6	1.0	6.40
66	23	25.54	2.54	9.1	1.0	6.40
67	22	24.59	2.59	8.5	1.0	6.41
68	21.06	23.7	2.64	8.0	1.0	6.42
69	20	22.7	2.7	7.4	1.0	6.43
70	19	21.76	2.76	6.9	1.0	6.44
71	18	20.83	2.83	6.4	1.0	6.45
72	17	19.9	2.9	5.9	1.0	6.46
73	25	27.44	2.44	10.2	1.1	6.43
74	24	26.49	2.49	9.6	1.1	6.44
75	23	25.54	2.54	9.1	1.1	6.45
76	22	24.59	2.59	8.5	1.1	6.45
77	21.06	23.7	2.64	8.0	1.1	6.46
78	20	22.7	2.7	7.4	1.1	6.47
79	19	21.76	2.76	6.9	1.1	6.48
80	18	20.83	2.83	6.4	1.1	6.49
81	17	19.9	2.9	5.9	1.1	6.50
82	25	27.44	2.44	10.2	1.2	6.47
83	24	26.49	2.49	9.6	1.2	6.48
84	23	25.54	2.54	9.1	1.2	6.48
85	22	24.59	2.59	8.5	1.2	6.49
86	21.06	23.7	2.64	8.0	1.2	6.50
87	20	22.7	2.7	7.4	1.2	6.51
88	19	21.76	2.76	6.9	1.2	6.52
89	18	20.83	2.83	6.4	1.2	6.53
90	17	19.9	2.9	5.9	1.2	6.54
91	25	27.44	2.44	10.2	1.3	6.50
92	24	26.49	2.49	9.6	1.3	6.51
93	23	25.54	2.54	9.1	1.3	6.52
94	22	24.59	2.59	8.5	1.3	6.53
95	21.06	23.7	2.64	8.0	1.3	6.54
96	20	22.7	2.7	7.4	1.3	6.55
97	19	21.76	2.76	6.9	1.3	6.55
98	18	20.83	2.83	6.4	1.3	6.57
99	17	19.9	2.9	5.9	1.3	6.58
100	25	27.44	2.44	10.2	1.4	6.53
101	24	26.49	2.49	9.6	1.4	6.54
102	23	25.54	2.54	9.1	1.4	6.55
103	22	24.59	2.59	8.5	1.4	6.56
104	21.06	23.7	2.64	8.0	1.4	6.57
105	20	22.7	2.7	7.4	1.4	6.58
106	19	21.76	2.76	6.9	1.4	6.59
107	18	20.83	2.83	6.4	1.4	6.60
108	17	19.9	2.9	5.9	1.4	6.61
109	25	27.44	2.44	10.2	1.5	6.56
110	24	26.49	2.49	9.6	1.5	6.57
111	23	25.54	2.54	9.1	1.5	6.58
112	22	24.59	2.59	8.5	1.5	6.59
113	21.06	23.7	2.64	8.0	1.5	6.60
114	20	22.7	2.7	7.4	1.5	6.61
115	19	21.76	2.76	6.9	1.5	6.62
116	18	20.83	2.83	6.4	1.5	6.63
117	17	19.9	2.9	5.9	1.5	6.64

Appendix B

Table A2. Various scenarios of the submarine at different speeds for the transverse motion.

Case	L (m)	L_{oa} (m)	D_S (m)	L/D_S	V_t (m/s)	$\text{Log}(R_{et})$
1	25	27.44	2.44	10.2	0.05	4.69
2	24	26.49	2.49	9.6	0.05	4.70
3	23	25.54	2.54	9.1	0.05	4.71
4	22	24.59	2.59	8.5	0.05	4.71
5	21.06	23.7	2.64	8.0	0.05	4.72
6	20	22.7	2.7	7.4	0.05	4.73
7	19	21.76	2.76	6.9	0.05	4.74
8	18	20.83	2.83	6.4	0.05	4.75
9	17	19.9	2.9	5.9	0.05	4.76
10	25	27.44	2.44	10.2	0.1	5.09
11	24	26.49	2.49	9.6	0.1	5.10
12	23	25.54	2.54	9.1	0.1	5.10
13	22	24.59	2.59	8.5	0.1	5.11
14	21.06	23.7	2.64	8.0	0.1	5.12
15	20	22.7	2.7	7.4	0.1	5.13
16	19	21.76	2.76	6.9	0.1	5.14
17	18	20.83	2.83	6.4	0.1	5.15
18	17	19.9	2.9	5.9	0.1	5.16
19	25	27.44	2.44	10.2	0.15	5.39
20	24	26.49	2.49	9.6	0.15	5.40
21	23	25.54	2.54	9.1	0.15	5.40
22	22	24.59	2.59	8.5	0.15	5.41
23	21.06	23.7	2.64	8.0	0.15	5.42
24	20	22.7	2.7	7.4	0.15	5.43
25	19	21.76	2.76	6.9	0.15	5.44
26	18	20.83	2.83	6.4	0.15	5.45
27	17	19.9	2.9	5.9	0.15	5.46
28	25	27.44	2.44	10.2	0.2	5.48
29	24	26.49	2.49	9.6	0.2	5.49
30	23	25.54	2.54	9.1	0.2	5.50
31	22	24.59	2.59	8.5	0.2	5.51
32	21.06	23.7	2.64	8.0	0.2	5.52
33	20	22.7	2.7	7.4	0.2	5.53
34	19	21.76	2.76	6.9	0.2	5.54
35	18	20.83	2.83	6.4	0.2	5.55
36	17	19.9	2.9	5.9	0.2	5.56
37	25	27.44	2.44	10.2	0.25	5.56
38	24	26.49	2.49	9.6	0.25	5.57
39	23	25.54	2.54	9.1	0.25	5.58
40	22	24.59	2.59	8.5	0.25	5.59
41	21.06	23.7	2.64	8.0	0.25	5.60
42	20	22.7	2.7	7.4	0.25	5.83
43	19	21.76	2.76	6.9	0.25	5.84
44	18	20.83	2.83	6.4	0.25	5.85
45	17	19.9	2.9	5.9	0.25	5.86
46	25	27.44	2.44	10.2	0.3	5.86
47	24	26.49	2.49	9.6	0.3	5.87
48	23	25.54	2.54	9.1	0.3	5.88
49	22	24.59	2.59	8.5	0.3	5.89
50	21.06	23.7	2.64	8.0	0.3	5.90
51	20	22.7	2.7	7.4	0.3	5.91
52	19	21.76	2.76	6.9	0.3	5.92
53	18	20.83	2.83	6.4	0.3	5.93
54	17	19.9	2.9	5.9	0.3	5.94

Table A2. Cont.

Case	L (m)	L_{oa} (m)	D_S (m)	L/D_S	V_t (m/s)	$\text{Log}(R_{ct})$
55	25	27.44	2.44	10.2	0.35	5.93
56	24	26.49	2.49	9.6	0.35	5.94
57	23	25.54	2.54	9.1	0.35	5.95
58	22	24.59	2.59	8.5	0.35	5.96
59	21.06	23.7	2.64	8.0	0.35	5.97
60	20	22.7	2.7	7.4	0.35	5.98
61	19	21.76	2.76	6.9	0.35	5.98
62	18	20.83	2.83	6.4	0.35	6.00
63	17	19.9	2.9	5.9	0.35	6.01
64	25	27.44	2.44	10.2	0.4	5.96
65	24	26.49	2.49	9.6	0.4	5.97
66	23	25.54	2.54	9.1	0.4	5.98
67	22	24.59	2.59	8.5	0.4	5.99
68	21.06	23.7	2.64	8.0	0.4	6.00
69	20	22.7	2.7	7.4	0.4	6.01
70	19	21.76	2.76	6.9	0.4	6.01
71	18	20.83	2.83	6.4	0.4	6.03
72	17	19.9	2.9	5.9	0.4	6.04
73	25	27.44	2.44	10.2	0.45	5.99
74	24	26.49	2.49	9.6	0.45	6.00
75	23	25.54	2.54	9.1	0.45	6.01
76	22	24.59	2.59	8.5	0.45	6.02
77	21.06	23.7	2.64	8.0	0.45	6.02
78	20	22.7	2.7	7.4	0.45	6.03
79	19	21.76	2.76	6.9	0.45	6.09
80	18	20.83	2.83	6.4	0.45	6.10
81	17	19.9	2.9	5.9	0.45	6.12
82	25	27.44	2.44	10.2	0.5	6.09
83	24	26.49	2.49	9.6	0.5	6.10
84	23	25.54	2.54	9.1	0.5	6.10
85	22	24.59	2.59	8.5	0.5	6.11
86	21.06	23.7	2.64	8.0	0.5	6.12
87	20	22.7	2.7	7.4	0.5	6.13
88	19	21.76	2.76	6.9	0.5	6.14
89	18	20.83	2.83	6.4	0.5	6.15
90	17	19.9	2.9	5.9	0.5	6.16

References

- Ćorak, M.; Šperanda, Z.; Čokić, J.; Parunov, J. Structural analysis of tourist submarine with acrylic hull. In *Sustainable Development and Innovations in Marine Technologies*, 1st ed.; Ergin, S., Guedes Soares, C., Eds.; CRC Press: London, UK, 2022. [\[CrossRef\]](#)
- Gatin, I.; Čokić, J.; Romić, D.; Parunov, J. CFD Study on the Influence of Exostructure Elements on the Resistance of a Submarine. *J. Mar. Sci. Eng.* **2022**, *10*, 1542. [\[CrossRef\]](#)
- Larsson, L.; Raven, H.C. *Ship Resistance and Flow, Principles of Naval Architecture Series*; SNAME: Alexandria, VA, USA, 2010.
- Wang, S.; Cui, L.; Wang, C.; Huang, S. Resistance performance of submarine under different traveling stations. In Proceedings of the World Automation Congress 2012, Puerto Vallarta, Mexico, 24–28 June 2012.
- Moonesun, M.; Javadi, M.; Charmdooz, P.; Mikhailovich, K.U. Evaluation of submarine model test in towing tank and comparison with CFD and experimental formulas for fully submerged resistance. *Indian J. Geo-Mar. Sci.* **2013**, *42*, 1049–1056.
- Sukas, O.F.; Kinaki, O.K.; Bal, S. Computation of total resistance of ships and a submarine by a RANSE based CFD. In Proceedings of the 2nd International Symposium on Naval Architecture and Maritime (INT-NAM 2014), Istanbul, Turkey, 23–24 October 2014.
- Moonesun, M.; Mikhailovich, Y.; Dalayeli, H. CFD Analysis on the Bare Hull Form of Submarines for Minimizing the Resistance. *Int. J. Marit. Technol.* **2015**, *3*, 1–16.
- Ahmed, Y.M. Viscous Resistance Prediction of a Tourist Submarine at Various Speeds. *Int. Rev. Mech. Eng.* **2016**, *10*, 247. [\[CrossRef\]](#)
- Shen, Y.T.; Hughes, M.J. A New Method for Scaling Submarine Resistance Model Data. In Proceedings of the SNAME 30th American Towing Tank Conference, West Bethesda, MD, USA, 4 October 2017.

10. Utina, M.R.; Murwatono, T.T.; Sadiyah, S. The Study on the Resistance Test Performance of BPPT Mini Submarine. In Proceedings of the SENTA 2018—The 3rd International Conference on Marine Technology, Surabaya, Indonesia, 5–6 December 2018.
11. Anh, T.P.; Vu Thanh, Q.; Ngo Van, H.; Le, Q.; Thi Thanh, H.P. Estimation Resistance of an Explorer Submarine. *J. Mech. Eng. Res. Dev.* **2020**, *43*, 264–271.
12. Liu, S.; He, G.; Wang, Z.; Luan, Z.; Zhang, Z.; Wang, W.; Gao, Y. Resistance and flow field of a submarine in a density stratified fluid. *Ocean. Eng.* **2020**, *217*, 107934. [[CrossRef](#)]
13. Chen, J.; Lv, B.; Peng, L.; Huang, B. Study on resistance characteristics of submarine near water surface. In Proceedings of the International Conference on Physics, Computing and Mathematical (ICPCM2021), Xiamen, China, 29–30 December 2022.
14. Takaaki, M.; Kai, F.; Koji, F. *Nonlinear Mode Decomposition with Convolutional Neural Networks for Fluid Dynamics*; Cambridge University Press: Cambridge, UK, 2019. [[CrossRef](#)]
15. Raissi, M.; Perdikaris, P.; Karniadakis, G.E. Physics-informed neural networks: A deep learning framework for solving forward and inverse problems involving nonlinear partial differential equations. *J. Comput. Phys.* **2019**, *378*, 686–707. [[CrossRef](#)]
16. Raissi, M.; Wang, Z.; Triantafyllou, M.S.; Em Karniadakis, G. Deep learning of vortex-induced vibrations. *J. Fluid Mech.* **2019**, *861*, 119–137. [[CrossRef](#)]
17. Brenner, M.P.; Eldredge, J.D.; Freund, J.B. Perspective on machine learning for advancing fluid mechanics. *Phys. Rev. Fluids* **2019**, *4*, 100501. [[CrossRef](#)]
18. Brunton, S.L.; Noack, B.R.; Koumoutsakos, P. Machine Learning for Fluid Mechanics. *Annu. Rev. Fluid Mech.* **2020**, *52*, 477–508. [[CrossRef](#)]
19. Saghi, H.; Mikkola, T.; Hirdaris, S. The influence of obliquely perforated dual baffles on sway induced tank sloshing dynamics. *Proc. Inst. Mech. Eng. Part M J. Eng. Marit. Environ.* **2020**, *235*, 905–920. [[CrossRef](#)]
20. OpenFoam. The Openfoam Foundation, User Guide. 10th July 2019. Available online: <http://openfoam.org> (accessed on 24 October 2022).
21. Allmendinger, E.E. *Submersible Vehicle System Design*; SNAME: Alexandria, VA, USA, 1990.
22. Dean, R.G.; Dalrymple, R.A. *Water Wave Mechanics for Engineers and Scientists*; World Scientific Publishing Company: Singapore, 1991.
23. Rahman, M.; Brebbia, C.A. *Advances in Fluid Mechanics IX*; WIT Press: Southampton, UK, 2012.
24. Jiang, Y. Computation of monthly mean daily global solar radiation in China using artificial neural networks and comparison with other empirical models. *Energy* **2009**, *34*, 1276–1283. [[CrossRef](#)]
25. Wang, Z.; Wang, F.; Su, S. Solar Irradiance Short-Term Prediction Model Based on BP Neural Network. *Energy Procedia* **2011**, *12*, 488–494. [[CrossRef](#)]
26. Zhang, Y.; Cui, N.; Feng, Y.; Gong, D.; Hu, X. Comparison of BP, PSO-BP and statistical models for predicting daily global solar radiation in arid Northwest China. *Comput. Electron. Agric.* **2019**, *164*, 104905. [[CrossRef](#)]
27. Du, B.; Lund, P.D.; Wang, J. Improving the accuracy of predicting the performance of solar collectors through clustering analysis with artificial neural network models. *Energy Rep.* **2022**, *8*, 3970–3981. [[CrossRef](#)]
28. Gu, J.; Wang, Z.; Kuen, J.; Ma, L.; Shahroudy, A.; Shuai, B.; Liu, T.; Wang, X.; Wang, G.; Cai, J.; et al. Recent advances in convolutional neural networks. *Pattern Recognit.* **2018**, *77*, 354–377. [[CrossRef](#)]
29. Zhang, Q.; Zhang, M.; Chen, T.; Sun, Z.; Ma, Y.; Yu, B. Recent advances in convolutional neural network acceleration. *Neurocomputing* **2019**, *323*, 37–51. [[CrossRef](#)]
30. Ma, C.; Jiang, L. Some research on Levenberg–Marquardt method for the nonlinear equations. *Appl. Math. Comput.* **2007**, *2*, 1032–1040. [[CrossRef](#)]
31. Moré, J.J. The Levenberg–Marquardt algorithm: Implementation and theory. In *Numerical Analysis*; Springer: Berlin/Heidelberg, Germany, 1978; pp. 105–116.
32. Pujol, J.J.G. The solution of nonlinear inverse problems and the Levenberg–Marquardt method. *Geophysics* **2007**, *72*, W1–W16. [[CrossRef](#)]
33. Transtrum, M.K.; Sethna, J.P. Improvements to the Levenberg–Marquardt algorithm for nonlinear least-squares minimization. *arXiv* **2012**, arXiv:1201.5885.
34. Haider, A.; Levenspiel, O. Drag coefficient and terminal velocity of spherical and non-spherical particles. *Powder Technol.* **1989**, *58*, 63–70. [[CrossRef](#)]
35. Hassan Khan, M.; Sooraj, P.; Sharma, A.; Agrawal, A. Flow around a Cube for Reynolds numbers between 500 and 55000. *Exp. Therm. Fluid Sci.* **2018**, *93*, 257–271. [[CrossRef](#)]
36. Kock, F.; Herwig, H. Local entropy production in turbulent shear flows: A high-Reynolds number model with wall functions. *Int. J. Heat Mass Transf.* **2004**, *47*, 2205–2215. [[CrossRef](#)]
37. Mikhailov, M.D.; Silva Freire, A.P. The drag coefficient of a sphere: An approximation using Shanks transform. *Powder Technol.* **2013**, *237*, 432–435. [[CrossRef](#)]
38. ISABELLA CLUSTER. Available online: <https://www.srce.unizg.hr/en/isabella-cluster> (accessed on 1 June 2022).
39. Streeter, V.L. *Fluid Mechanics*, 3rd ed.; McGraw-Hill: New York, NY, USA, 1962.

-
40. McElroy, P.D.; Bibang, H.; Emadi, H.; Kogolu, Y.; Hussain, A.; Watson, M.C. Artificial neural network (ANN) approach to predict unconfined compressive strength (UCS) of oil and gas well cement reinforced with nanoparticles. *J. Nat. Gas Sci. Eng.* **2021**, *88*, 103816. [[CrossRef](#)]
 41. Stathakis, D. How many hidden layers and nodes? *Int. J. Remote Sens.* **2009**, *30*, 2133–2147. [[CrossRef](#)]